J Solid State Electrochem (2005) 9: 684–690
DOI 10.1007/s10008-004-0643-5

ORIGINAL PAPER

Francisco Vicente · Joan Gregori
Jose Juan García-Jareño · David Giménez-Romero

Cyclic voltammetric generation and electrochemical quartz crystal microbalance characterization of passive layer of nickel in a weakly acid medium

Received: 2 July 2004 / Revised: 12 July 2004 / Accepted: 5 November 2004 / Published online: 5 May 2005

Abstract The electrochemical quartz crystal microbalance results show that nickel electrodissolution and nickel passivation occur simultaneously. Besides, the anodic transferred charge decreases and the passive layer thickness increases with the number of successive voltammetric cycles. Mass balances across the metal/passive layer/solution have been done from the instantaneous F(dm/dQ) function. A dynamic process for generation of an inner NiO and a $Ni(OH)_2$ outer passive layers is suggested.

Keywords Nickel · Anodic dissolution · Passivation · Electrochemical quartz crystal microbalance (EQCM)

Introduction

Technological metals such as Zn, Cu and Ni have been the subject of many researches related to dissolution and passivation mechanism in acid medium by means of different electrochemical techniques [1–17]. The obtained EIS spectra of Zn in a weakly acid medium [4–6] were consistent with an electrodissolution process according to two consecutive single-electron transfers followed by a mass transfer step. However, in the case of nickel, several points are yet unclear due to the strong tendency for self-passivation of nickel [14]. This tendency should prove more pronounced in weakly acid or alkaline media [18–20] and it is affected drastically to a great extent by anions [21] and other experimental conditions [11, 12]. Under voltammetric conditions the active–passive transition is characterized by one or more anodic peaks at which the formation of a film of nickel hydroxide, as the first stage of nickel passivity, is considered [8, 22]. From a technological point of view, the formation of passive layers on nickel has great importance due to their use in rechargeable alkaline batteries [23], cathodes in fuel cells [24] and electrocatalysts for oxygen evolution [25]. Moreover, nickel is an element included in many alloys to increase their corrosion resistance [26–28]. It is commonly accepted that the passive layer on nickel has a bilayer structure with an inner layer of crystalline NiO and an hydrated outer layer of $Ni(OH)_2$ [29, 30]. The XPS results of Scherer et al. [30], are consistent, at acid pH, with a bilayer structure for the nickel passive layer, with an inner crystalline layer of NiO with a thickness between 1.4 and 4.7 nm, and an amorphous outer layer of $Ni(OH)_2$.

Quartz crystal microbalance (QCM) in combination with the cyclic voltammetry technique provides important information about the mechanism and the stoichiometry in the nickel dissolution and deposition process at pH ≈2.5 [17] by means of the measurement of the instantaneous mass/charge ratio function, defined as [4]:

$$F\frac{\mathrm{d}m}{\mathrm{d}Q} = \sum_i \frac{\mathrm{MW}_i}{n_i}\gamma_i \quad \pm \text{contribution of mass changes due to uncharged species} \tag{1}$$

where MW_i is the molecular mass of a species i, which interchanges n_i electrons, γ_i is the charge ratio due to process i, and F is the Faraday constant.

According to the Sauerbrey's equation [31], the mass changes on the electrode surface are related to the resonance frequency changes:

$$\Delta f = -\frac{2f_0^2}{A\sqrt{E_y\rho}}\Delta m_e \tag{2}$$

where ρ is the quartz density and E_y is the stretch constant of quartz. f_0 is the base resonance frequency.

This work is focused to study the process of formation of passive layers on nickel in weakly acid media

F. Vicente (✉) · J. Gregori · J. J. García-Jareño
D. Giménez-Romero
Laboratory of Electrochemistry,
Department of Physical Chemistry,
University of Valencia, C/Dr. Moliner 50,
46100 Burjassot, Spain
E-mail: Francisco.Vicente@uv.es
Fax: +34-963544564

(pH ≈5), at the same medium in which zinc shows only anodic dissolution but not passivation in the absence of oxygen [4]. The balance of mass and instantaneous values of $F\frac{dm}{dQ}$ function are analyzed in order to understand their relation with the shape of successive cyclic voltammograms of nickel electrode in this medium.

Experimental

All EQCM experiments were carried out in a typical three-electrodes cell at these conditions: 0.32 M H_3BO_3, 0.26 M NH_4Cl, 1.33 M Na_2SO_4, pH = 5.1 and $T = 298$ K.

The potential was measured versus the Ag/AgCl/KCl (sat.) reference electrode. A platinum grid was used as an auxiliary electrode. Solutions were prepared from Na_2SO_4 (Sigma, a.g.), H_3BO_3 (R.P. Normapur, a.g.), NH_4Cl (Panreac, a.g.), with distilled and double deionized water (MilliQ).

For EQCM experiments, the working electrodes were made from a quartz sheet (quartz was supplied by Matel–Fordahl) embedded between two pieces of gold connected to a resonance circuit. The resonance frequency of the quartz at air was 6 MHz. One of the pieces of gold serves as an electrical surface in contact with the electrolyte. The electrical area was 0.228 cm^2 and the effective mass area was 0.196 cm^2. Nickel electrodeposits were obtained by means of a potentiostatic method in a 0.245 M K_2SO_4 (Probus, a.g.), 0.005 M H_2SO_4 (Merk, a.g.) and 0.001 M $NiSO_4{\cdot}6H_2O$ (Scharlau, a.g.) medium prepared with distilled and double deionized water (MilliQ) pH = 2.72, $T = 298$ K. A potential E = −1,450 mV (vs. SSE) was applied for 5 min, and this process was repeated ten times at the same potential. In this way, the calculated mass density on the electrode surface is 23.7 μg cm^{-2}. From this value and the nickel density value, the deposit thickness can be estimated, $\delta = 2.7\times10^{-8}$ m < 2×10^{-7} m, and then no nonideal contributions are expected and Sauerbreys' equation applies [31]. The successive potential sweeps were carried out in the [−500,500] mV (vs. Ag/AgCl/KCl (sat.)), potential interval at 20 mV/s. Before starting the potential sweep the potential was kept constant at −500 mV for 1 min. The electrolyte was bubbled for 5 min with Ar (Air Liquide) so as to remove the dissolved oxygen and all the measurements were taken under inert atmosphere and at constant and controlled temperature $T = 298.0$ K. The microbalance was an UPR15/RT0100 (UPR of the CNRS). The resonance frequency of quartz was measured with a Fluke PM6685. The current in the auxiliary electrode was measured with a Keithley PM2000 multimeter. The potential was applied with a 263A EG&G PAR Potentiostat. The whole system was controlled by a GPIB board. The EQCM was calibrated by means of a galvanostatic Cu deposition [32]. The experimental Sauerbrey constant was 9.50×10^7 Hz g^{-1}.

Microanalysis (EDX) and electron scan microscopy (SEM) were performed by means of a Phillips XL30 ESEM.

Experimental results and discussion

Instantaneous mass–charge ratio during successive voltammetric cycles

Figure 1 shows the successive cyclic voltammograms (scan rate 20 mV/s) and the successive mass changes for a nickel deposit of 23.7 μg cm^{-2} in the [−500,500] mV (vs. Ag|AgCl|KCl (sat.)) potential window.

During the successive anodic scans a considerable loss of mass and charge transference takes place in the anodic potential interval. These values can be seen in Table 1 as a function of the number of cycles, together with the calculated mass/charge ratio $F\Delta m/\Delta Q$ which also tends to decrease with the number of cycles. If it is considered that the total mass loss, after the 20th successive cycles (6.2 μg cm^{-2}), is smaller than the electrodeposited mass of nickel (23.7 μg cm^{-2}), the evolution of all these parameters can be explained if a progressive nickel passivation takes place. Moreover, the total anodic charge after the 20th successive potential cycle is 39.4 mC cm^{-2}, to which an overall mass of 11.8 μg cm^{-2} of oxidized nickel should correspond, if it is considered that anodic charge is due to the reaction of a mole of Ni for each two electrons. That way, after the successive potential cycles a relatively great amount of metallic nickel (about 50%) remains on the electrode surface.

Finally, in the cathodic potential interval no appreciable mass change is recorded, and it can be considered that the passive film formed is apparently stable, but the overlapping of hydrogen evolution reaction makes the

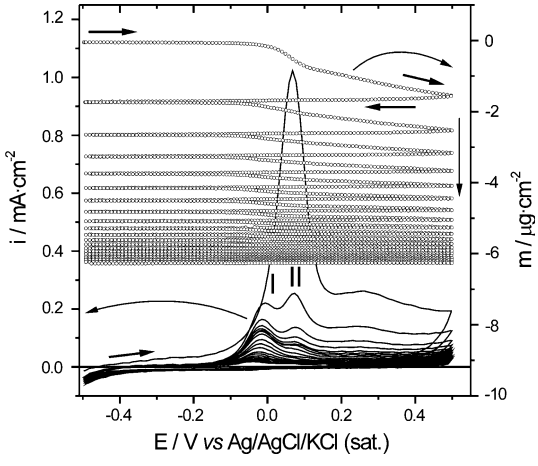

Fig. 1 Successive voltammograms and mass changes in the [−500,500] mV potential range. *Arrows* indicate the sense of the successive scans. 20 cycles, scan rate 20 mV/s. 0.32 M H_3BO_3, 0.26 M NH_4Cl, 1.33 M Na_2SO_4 pH = 5.1 $T = 298$ K

Table 1 Experimental anodic charge, ΔQ, mass variation in the anodic scan, Δm, and mass/charge ratio, $F\,\Delta m/\Delta Q$, as a function of the number of cycles

Cycle	ΔQ mC cm^{-2}	Δm μg cm^{-2}	$F\,\Delta m/\Delta Q$ g mol^{-1}
1	10.8	−1.6	−14
2	5.0	−0.9	−17
3	3.3	−0.6	−16
5	2.3	−0.4	−15
10	1.3	−0.2	−11
15	0.7	−0.07	−10
20	0.4	−0.03	−6

Same experimental conditions as in Fig. 1. ΔQ values were obtained from the area under the voltammogram between [−200,500] mV in the anodic sense

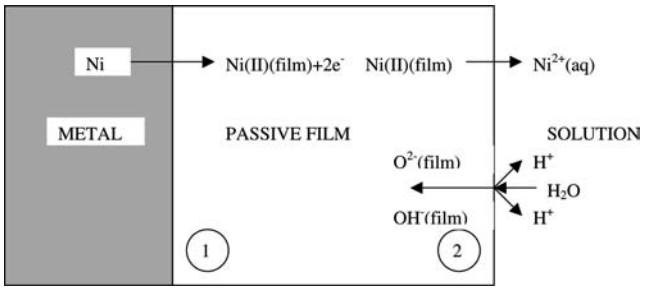

Fig. 3 Scheme of the Ni/passive layer/electrolyte system. *1* and *2* represent the Ni/passive layer and passive layer/electrolyte interfaces, respectively. Probably a NiO thin layer (near a monolayer) is formed between the Ni (metal) and the $Ni(OH)_2$ passive layer in contact with the solution

interpretation of EQCM results obtained at this range of potential.

The study of the instantaneous mass/charge ratio, $F\,dm/dQ$ function, has turned out to be very useful in the study of metal dissolution process [4, 32], and charge transport in polymer modified electrodes [33]. In Fig. 2a, the instantaneous mass/charge ratio values are represented for the first anodic scan.

As can be seen in Fig. 2a, at the beginning of the anodic peak $F\,dm/dQ = -17$ g mol^{-1}. This value is lower than the expected theoretical value of -29 g mol^{-1} for a simple electro-dissolution process such as:

$$Ni \rightarrow Ni^{2+} + 2e^- \quad (3)$$

This discrepancy can be explained if a passivation process is considered. If passivation process proceeds according to [8, 22]:

$$Ni + 2OH^- \rightarrow Ni(OH)_2 + 2e^- \quad (4)$$

from $F\,dm/dQ$ definition, the charge fraction due to electrodissolution and passivation process can be calculated for the first voltammetric cycle, according to:

$$F\frac{dm}{dQ}\bigg|_{exp} = \gamma_1 F\frac{dm}{dQ}\bigg|_{dissolution} + \gamma_2 F\frac{dm}{dQ}\bigg|_{passivation} \quad (5)$$

where γ_1 is the charge fraction due to electrodissolution process and γ_2 is the charge fraction due to passivation process, and $F\frac{dm}{dQ}\Big|_{dissolution} = -29\,g\,mol^{-1}, F\frac{dm}{dQ}\Big|_{passivation} =$ $17\,g\,mol^{-1}$ (if passivation takes place according reaction (Eq. 4)). The intensity components for each electrochemical process ($i_1 = i\,\gamma_1$ for electrodissolution, and $i_2 = i\gamma_2$ for passivation) can be calculated from Eq. 5 for the first cycle in the anodic potential interval, and it is found that nickel electrodissolution and nickel passivation proceed simultaneously in the whole anodic potential interval, and these processes cannot be well separated in these experimental conditions. Hence, the experimental $F\,dm/dQ$ value suggests that about 25% of the charge is associated to passivation process at the beginning of the anodic peak. As the potential becomes more anodic, $F\,dm/dQ$ value increases (due to the − sign) up to a value of -12 g mol^{-1} at peak potential. This increase is accompanied by an increase in current due to an enhanced nickel electrodissolution as the potential increases (see Fig. 2a between 0.0 V and 0.1 V interval of potential). That way, the increase amount of Ni^{2+} on the electrode surface should produce a precipitation of $Ni(OH)_2$ since this hydroxide has a low solubility constant and a greater passivation degree is reached. The experimental $F\,dm/dQ$ value at peak potential suggests that about 35% of the charge is associated to passivation process. Subsequently, current intensity rapidly decreases and this fact produces a decrease in the $F\,dm/dQ$ value until an almost constant value is reached in passivity potential interval.

As can be seen in Fig. 2b, the initial anodic peak is divided into two anodic peaks, peak I and peak II. In Fig. 2b the voltammogram and the $F\,dm/dQ$ function for the second cycle are plotted versus potential. A

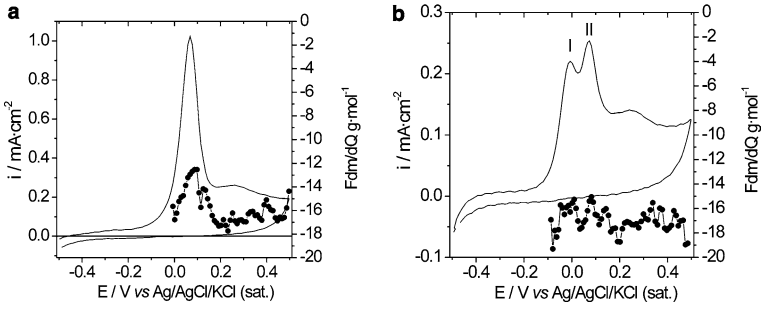

Fig. 2 Voltammogram and instantaneous mass/charge ratio function. **a** First cycle and **b** second cycle. Same experimental conditions as in Fig. 1

constant value of about -17 g mol^{-1} along the whole anodic potential interval is observed, and the formation of the passive layer during the first cycle causes the peak multiplicity [8, 22, 34]. Also experimentally it is observed that, with the number of cycles, $F\,\mathrm{d}m/\mathrm{d}Q$ values increase in passivity potential interval [0.1,0.4] V and anodic peak II appears as a shoulder in the voltammetric curve and only peak I is clearly defined, although peak intensity is strongly decreased after the tenth cycle.

Mass balance at the interfaces

According to the previously discussed results, a well-formed passive layer after the first cycle is expected. Then, after the first cycle, the physical situation may correspond to the scheme of Fig. 3 [35–37], where the nickel deposit is covered by a passivation layer.

At the interface (1) metal/passive layer, the following process takes place:

$$\mathrm{Ni} \rightarrow \mathrm{Ni(II)\,(film)} + 2e^- \tag{6}$$

to which a charge ΔQ corresponds. ΔQ corresponds to the measured charge variations. This electrical charge is associated with an equivalent mass variation $\Delta m_1 = (M/nF)\,\Delta Q$ where $n = 2$. At the interface (2) passive layer/solution a nonoxidative dissolution of nickel ions takes place, according to:

$$\mathrm{Ni(II)\,(passive\,layer)} \rightarrow \mathrm{Ni}^{2+}\ \mathrm{(solution)} \tag{7}$$

to which a mass variation Δm_2 corresponds. Moreover, the reaction of electrolyte anions takes place at the interface (2), fundamentally oxygen or hydroxyl ions:

$$\mathrm{H_2O} \rightleftarrows \mathrm{O^{2-}(passive\,layer)} + 2\mathrm{H^+} \tag{8}$$

$$\mathrm{H_2O} \rightleftarrows \mathrm{OH^-(passive\,layer)} + \mathrm{H^+} \tag{9}$$

to which a mass variation Δm_O corresponds. Note that, by definition, Δm_2 is a negative magnitude and Δm_O a positive one. The measured mass variation by the QCMB is given by:

$$\Delta m = \Delta m_2 + \Delta m_O \tag{10}$$

and the mass change of the passive layer is given by:

$$\Delta m_{film} = \Delta m_1 + \Delta m_2 + \Delta m_O \tag{11}$$

If the nickel passive layer has an stoichiometry NiX_γ where X represents O^{2-} or OH^- species, the mass change associated with reactions (Eq. 8 or Eq. 9) is:

$$\frac{\Delta m_O}{M_O} = \frac{\gamma}{M}(\Delta m_1 + \Delta m_2) \tag{12}$$

where M_O represents the molecular mass of O^{2-} or OH^-, $M = 59$ g mol^{-1} is the nickel molecular mass, and γ represents the stoichiometric coefficient. From Eqs. 10 and 12, the differential measured mass variation, d m, can be expressed as:

$$\mathrm{d}m = \frac{\gamma M_O}{M}\mathrm{d}m_1 + \left(1 + \frac{\gamma M_O}{M}\right)\mathrm{d}m_2 \tag{13}$$

and, consequently, the $F\,\mathrm{d}m/\mathrm{d}Q$ function is given by:

$$F\frac{\mathrm{d}m}{\mathrm{d}Q} = F\frac{\gamma M_O}{M}\frac{\mathrm{d}m_1}{\mathrm{d}Q} + \frac{M}{n}\left(1 + \frac{\gamma M_O}{M}\right)\frac{\mathrm{d}m_2}{\mathrm{d}m_1} \tag{14}$$

and:

$$\left|\frac{\mathrm{d}m_2}{\mathrm{d}m_1}\right| = \frac{\frac{\gamma M_O}{M}F\frac{\mathrm{d}m_1}{\mathrm{d}Q} - F\frac{\mathrm{d}m}{\mathrm{d}Q}}{\frac{M}{n}\left(1 + \frac{\gamma M_O}{M}\right)} \tag{15}$$

The ratio d m_2/d m_1 indicates what fraction of cations Ni^{2+} formed at the interface (1) dissolve into the electrolyte at the interface (2), and the $F\,\mathrm{d}m/\mathrm{d}Q$ function allows to obtain a punctual measure of such ratio. The obtained constant value $F\,\mathrm{d}m/\mathrm{d}Q = -18$ g mol^{-1} for the second cycle (see Fig. 2b), implies that the d m_2/d m_1 ratio is 0.76 if it is considered that the passive layer is formed by $Ni(OH)_2$. The same constant $F\,\mathrm{d}m/\mathrm{d}Q$ value is obtained for the third, fourth and fifth cycles in all anodic potential interval, and the same analysis as in the previous cases is applicable. In this sense, $F\,\mathrm{d}m/\mathrm{d}Q$ expression can be written as [4, 32]:

$$F\frac{\mathrm{d}m}{\mathrm{d}Q} = F\frac{\mathrm{d}m/\mathrm{d}t}{I} \tag{16}$$

and consequently an $F\,\mathrm{d}m/\mathrm{d}Q$ constant value implies that the d m/d t curve must be proportional to the I curve.

In Fig. 4 the $-$d m/d t versus E plots are plotted for the first (Fig. 4a) and second (Fig. 4b) cycles, together with the voltammetric curves. A close proportionality between the curves for both cycles is observed throughout the anodic potential interval. Another

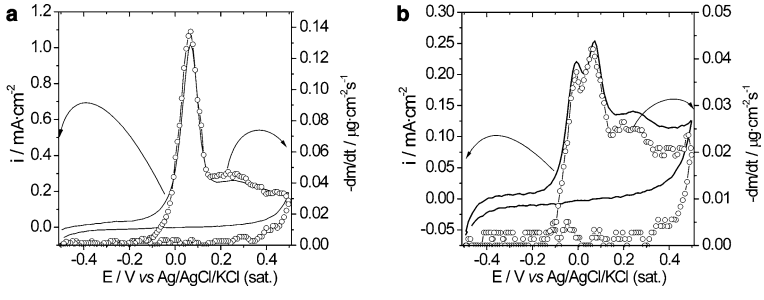

Fig. 4 Comparison between voltammograms (*solid line*) and the $-$d m/d t function (*empty circles*). **a** First cycle and **b** second cycle. Same experimental conditions as in Fig. 1

Table 2 Experimental mass and charge variations, Δm and ΔQ, respectively, for the anodic potential interval, as a function of the number of cycles

Δm_{film} and $\Delta\delta_{film}$ represent the film mass increase and the film thickening, respectively. They are calculated according to Eqs. 17 and 18, respectively

Cycle	Δm (oxidation) μg cm^{-2}	ΔQ (oxidation) mC cm^{-2}	Δm_{film} μg cm^{-2}	$\Delta\delta_{film}$ nm
1	−1.64	10.8	–	–
2	−0.87	5.02	0.64	2.5
3	−0.56	3.32	0.44	1.7
5	−0.36	2.29	0.33	1.3
10	−0.15	1.26	0.24	0.9
15	−0.07	0.67	0.13	0.5
20	−0.03	0.45	0.11	0.4

interesting fact is related to the value of the $-\mathrm{d}\,m/\mathrm{d}\,t$ curve in hydrogen evolution potential interval during the cathodic scan. A zero value of $-\mathrm{d}\,m/\mathrm{d}\,t$ is obtained, since the hydrogen evolution does not imply mass changes.

From the fifth cycle on, the behavior of the $F\,\mathrm{d}m/\mathrm{d}Q$ function is quite repetitive with the number of cycles: at the beginning of anodic peak *I*, it has a value close to -20 g mol^{-1} then it increases until a constant value is reached in the [0,400] mV potential interval (which includes anodic peak II), and finally a further decrease in the $F\,\mathrm{d}m/\mathrm{d}Q$ value until -20 g mol^{-1} is observed at 500 mV. The constant value reached in the [0,400] mV potential interval tends to increase with the number of cycles. This increase in the $F\,\mathrm{d}m/\mathrm{d}Q$ value in the passivity potential interval with the number of cycles should cause the decrease of $\mathrm{d}\,m_2/\mathrm{d}\,m_1$ ratio, and a more stable passive film is reached with the number of cycles. All these experimental results are consistent with a greater passivation degree as the number of cycles increases. However, a $F\,\mathrm{d}m/\mathrm{d}Q$ value, close to -20 g mol^{-1} at 500 mV is observed from the fifth cycle which coincides with a rise of the anodic current. This value implies an increase of the $\mathrm{d}\,m_2/\mathrm{d}\,m_1$ ratio which could be associated with the phenomenon of the transpassive dissolution of nickel.

The mass change of the passive layer can be written as:

$$\Delta m_{film} = \Delta m + \frac{M}{nF}\Delta Q \tag{17}$$

and from this value the passive layer thickening is given by:

$$\Delta\delta_{film} = \frac{\Delta m_{film}}{\rho_{film}} \tag{18}$$

where ρ_{film} represents the density of the formed passive layer. Δm, ΔQ_1, Δm_{film} and $\Delta\delta_{film}$ are represented in Table 2 as a function of the number of cycles for the whole anodic potential interval, and $\Delta\,\delta_{film}$ is calculated considering that a $Ni(OH)_2$ passive layer is formed, and for a compact $Ni(OH)_2$ structure $\rho_{film} = 2.6$ g cm^{-3}. In Table 3 the same values are represented but Δm, ΔQ_1 are calculated considering only mass variations and the charge under the anodic peak I. The obtained $\Delta\,\delta_{film}$ (peak I) value is consistent with the formation of few monolayers of passive layer.

The potential difference between peak I and peak II is close to 85 mV at 298 K. If it is considered that this difference corresponds to the existence of two different ways of oxidation of Ni, the maximum standard free enthalpy between both the processes should be:

$$\Delta G^0 = \Delta G^0_{peakII} - \Delta G^0_{peakI} \approx -2F\Delta E_p = -17\,\mathrm{kJ}\cdot\mathrm{mol}^{-1} \tag{19}$$

and according to thermodynamic data [38], this ΔG^0 obtained value corresponds to the difference between the standard free energies of formation ΔG^0_j of NiO (-211.10 kJ mol^{-1}) and $NiOH^+$ (-227.2 kJ mol^{-1}) from Ni metal. Accordingly, the generated passive layer most probably has a bilayer structure from the second cycle, with an inner NiO monolayer and an outermost hydrated $Ni(OH)_2$ layer, and in accordance with other experimental results [30, 39]. In this sense, peak I should correspond apparently to the formation of a few monolayers of NiO from the Ni(II) formed at the nickel/passive layer interface, and peak II should correspond to the formation of $Ni(OH)_2$ through $NiOH^+$ intermediate.

Finally, Eq. 13 can be written as:

$$\frac{\mathrm{d}m}{\mathrm{d}t} = \frac{\gamma M_O}{M}\frac{\mathrm{d}m_1}{\mathrm{d}t} + \left(1+\frac{\gamma M_O}{M}\right)\frac{\mathrm{d}m_2}{\mathrm{d}t} = \frac{\gamma M_O}{nF}i + \left(1+\frac{\gamma M_O}{M}\right)\frac{\mathrm{d}m_2}{\mathrm{d}t} \tag{20}$$

where $i = \mathrm{d}\,Q/\mathrm{d}\,t$ is the measured intensity, $n = 2$ and $M_O = 17$, $\gamma = 2$ if a $Ni(OH)_2$ passivation layer is considered. Then:

$$\frac{\mathrm{d}m_2}{\mathrm{d}t} = \frac{\frac{\mathrm{d}m}{\mathrm{d}t} - \frac{\gamma M_O}{nF}i}{\left(1+\frac{\gamma M_O}{M}\right)} \tag{21}$$

which is a measure of the mass loss rate at the interface passive layer/electrolyte. Moreover:

$$\frac{\mathrm{d}m_1}{\mathrm{d}t} = \frac{M}{nF}\frac{\mathrm{d}Q}{\mathrm{d}t} = \frac{M}{nF}i \tag{22}$$

where i is the measured density current.

In Table 4, $(-\mathrm{d}m/\mathrm{d}t)$, $(-\mathrm{d}m_1/\mathrm{d}t)$ and $(-\mathrm{d}m_2/\mathrm{d}t)$ values are represented as a function of the number of cycles, at two different peak potentials, $E_1 = -14$ mV (anodic peak potential I) and $E_2 = 270$ mV (within passivity

Table 3 Experimental mass and charge variations, Δ m (peak I) and Δ Q (peak I), respectively, for anodic peak I, as a function of the number of cycles

Cycle	Δ m (peak I) μg cm^{-2}	Δ Q (peak I) mC cm^{-2}	Δ m_{film} (peak I) μg cm^{-2}	Δ δ_{film} (peak I) nm
1	–	–	–	–
2	−0.24	1.46	0.21	0.31
3	−0.17	0.99	0.13	0.19
5	−0.16	0.90	0.12	0.18
10	−0.10	0.63	0.09	0.13
15	−0.04	0.28	0.05	0.07
20	−0.01	0.16	0.04	0.07

Δm_{film} (peak I) and $\Delta\delta_{film}$ (peak I) represent the film mass increase and the film thickening, respectively. They were calculated according Eqs. 17 and 18, respectively. Δ m (peak I) and Δ Q (peak I) values were calculated as twice the area under $-dm/dt$ and voltammetric curves, respectively, up to anodic peak I potential. Δ δ_{film} (peak I) were calculated by considering ρ (NiO) = 6.8 g·cm^{-3}

Table 4 $-\mathrm{d}\,m/\mathrm{d}\,t$, $-\mathrm{d}\,m_1/\mathrm{d}\,t$ and $-\mathrm{d}\,m_2/\mathrm{d}\,t$ values as a function of the number of cycles for $E_1 = -14$ mV (anodic peak I potential) and $E_2 = 270$ mV, calculated from Eqs. 21 and 22 and $-\mathrm{d}\,m/\mathrm{d}\,t$ curves

Cycle	$\left\lvert\frac{-\mathrm{d}m}{\mathrm{d}t}\right\rvert_{E1}$ μg s^{-1} cm^{-2}	$\left\lvert\frac{-\mathrm{d}m_1}{\mathrm{d}t}\right\rvert_{E1}$ μg s^{-1} cm^{-2}	$\left\lvert\frac{-\mathrm{d}m_2}{\mathrm{d}t}\right\rvert_{E1}$ μg s^{-1} cm^{-2}	$\left\lvert\frac{-\mathrm{d}m}{\mathrm{d}t}\right\rvert_{E2}$ μg s^{-1} cm^{-2}	$\left\lvert\frac{-\mathrm{d}m_1}{\mathrm{d}t}\right\rvert_{E2}$ μg s^{-1} cm^{-2}	$\left\lvert\frac{-\mathrm{d}m_2}{\mathrm{d}t}\right\rvert_{E2}$ μg s^{-1} cm^{-2}
2	0.037	0.067	0.048	0.025	0.043	0.031
3	0.027	0.049	0.035	0.015	0.028	0.019
4	0.024	0.043	0.031	0.014	0.021	0.014
5	0.022	0.040	0.029	0.012	0.016	0.012
6	0.020	0.040	0.027	0.005	0.015	0.009
7	0.020	0.037	0.026	0.004	0.012	0.007
8	0.020	0.034	0.025	0.004	0.011	0.007
9	0.013	0.028	0.018	0.003	0.009	0.005
10	0.012	0.024	0.016	0.003	0.008	0.005

potential interval). As can be seen in Table 4, these values tend to decrease with the number of cycles, fundamentally in passivity potential interval, which indicates that the passive layer becomes more stable and the protection against corrosion is more effective as the number of cycles increase. In all cases, the derivatives d m/d t or d m/d E allow to compare the rate of the mass transfer steps at different potentials. It is interesting to point out that the ratios of d m_2/d t and d m_1/d t and the decrease with the number of cycles are almost the same (between 0.72 and 0.62) for the present peak I and the passive range potentials indicating that the formation of the film is mainly due to a precipitation process under this experimental generation of the passive layer. However, the capacitive effects associated with the passive layer affect significantly all measurements related to the current intensity or the charge transferred after the tenth cycle.

The methodological use of d m/d t and dm/dQ derivatives could be result in promising possibilities to understand other interesting results obtained by means of EQCM technique at basic media [40] as well as in more acid media [17] if the changes of mass comply to Sauerbrey's equation.

Conclusion

The functions F(d m/d Q) and (d m/d t) obtained from voltammograms combined with QCM measurements are very useful to explain the anodic dissolution of nickel.

From the aforementioned results it is possible to draw the dynamic process of the both simultaneous dissolution and passivation processes of nickel at weakly acid media. The development of the experiments could be like this:

1. At the beginning, the electrochemical dissolution takes place on the interface metal/solution. Ni(II), generated on the surface, yields Ni^{2+} within the solution.
2. The process of formation of Ni(II) on the Ni surface is strongly affected by the presence of the anions on the surface. Subsequently, a $Ni(OH)_2$ layer is formed from the Ni^{2+}, placed near the electrode (solubility constant $K_s \approx 5\ 10^{-16}$ [41]).
3. Those two previous paths cause a passivation layer generated during the first voltammetric cycle. Then, the formation of $Ni(OH)_2$ is hindered with respect to the formation of a monolayer of NiO inside the previous passive layer due to the fact that the first passive layer of $Ni(OH)_2$ acts as a barrier that difficult the direct reaction of OH^- anions with Ni(II) formed on the Ni metal. This fact is observed by the recording of two voltammetric peaks in the second voltammogram. Peak II recorded at a higher overpotential corresponds to the formation of $Ni(OH)_2$ across an intermediate species $NiOH^+$, which reacts with the OH^- of the solution phase for yielding new layers of $Ni(OH)_2$. The oxidation of the surface atoms of the metal yields NiO (peak I), which transforms continuously to $Ni(OH)_2$ via $NiOH^+$.

4. This passive layer dissolves continuously, but it is increasingly more difficult for (OH^-) to reach the inner layer. Consequently, successive voltammetric cycles cause the formation of a passive layer that hinders the dissolution of the nickel. This passive layer shows a homogeneous and amorphous morphology without appreciable amounts of N, B or S atoms in EDX microanalysis.

Acknowledgements This work has been supported by Spanish Ministery of Science and Technology (Project CICyT-Mat/2000-011-P4). D. Giménez-Romero acknowledges a Fellowship from the Regional Gobernment Generalitat Valenciana (FPI program). J. Gregori acknowledges a Fellowship from the Spanish Education Ministery (FPU program). J.J. García-Jareño acknowledges their position (''Ramón y Cajal'' Program) to the Spanish Ministery of Science and Technology.

References

1. Itagaki M, Tagaki M, Watanabe K (1996) Corros Sci 38:1109
2. Bund A, Schwitzgebel G (2000) Electrochim Acta 45:3703
3. Cachet C, Ganne F, Maurin G, Petitjean J, Vivier V, Wiart R (2001) Electrochim Acta 47:509
4. Giménez-Romero D, García-Jareño JJ, Vicente F (2003) J Electroanal Chem 558:25
5. Giménez-Romero D, García-Jareño JJ, Vicente F (2003) Electrochem Commun 5:722
6. Giménez-Romero D, García-Jareño JJ, Vicente F (2004) J Electroanal Chem 572:235
7. Real SG, Vilche JR, Arvía AJ (1980) Corros Sci 20:563
8. Barbosa MR, Real SG, Vilche JR, Arvía AJ (1988) J Electrochem Soc 135:1077
9. MacDougall B (1979) J Electrochem Soc 126:919
10. Abd El Rehim SS, Abd El Wahaab SM, Abd El Meguid EA (1986) Surf Coat Technol 29:325
11. Jouanneau A, Keddam M, Petit MC (1976) Electrochim Acta 21:287
12. Barbosa MR, Bastos JA, Gacía-Jareño JJ, Vicente F (1998) Electrochim Acta 44:957
13. Keddam M, Takenouti H, Yu N (1985) J Electrochem Soc 132:2561
14. Keddam M (1995) Corrosion mechanism in theory and practice. In: Marcus P, Oudar J (eds). Marcell Dekker, New York, pp 55–122
15. Itagaki M, Nakazawa H, Watanabe K, Noda K (1997) Corros Sci 39:901
16. Gabrielli C, Moçotéguy P, Perrot H, Wiart R (2004) J Electroanal Chem 572:367
17. Gregori J, García-Jareño JJ, Giménez D, Vicente F (2005) J Solid State Electr 9:83
18. D'Alkaine CV, Santanna MA (1998) J Electroanal Chem 457:5
19. D'Alkaine CV, Santanna MA (1998) J Electroanal Chem 457:13
20. Leroy L, Girault P, Grosseau-Poussard JL, Dinhut JF (2002) Nucl Instrum Method B 148:49
21. Armstrong RD, Thirsk HR (1972) Electrochim Acta 17:171
22. Real SG, Barbosa MR, Vilche JR, Arvía AJ (1990) J Electrochem Soc 137:1696
23. De Souza LMN, Kong FP, McLarnon FR, Muller RH (1997) Electrochim Acta 42:1253
24. Kim SG, Yoon SP, Han J, Nam SW, Lim TH, Oh IH, Hong SA (2004) Electrochim Acta 49:3081
25. Rashkova V, Kitova S, Konstantinov I, Vitanov T (2002) Electrochim Acta 47:1555
26. Martini EMA, Amaral ST, Müller IL (2004) Corros Sci (in press)
27. Marcus P (1998) Electrochim Acta 43:109
28. Gildenpfennig A, Gramberg U, Hohlneicher G (2003) Corros Sci 45:575
29. Marcus P, Oudar J, Olefjord I (1979) J Microsc Spectrosc Electron 4:63
30. Scherer J, Ocko BM, Magnussen OM (2003) Electrochim Acta 48:1169
31. Sauerbrey G (1959) Z Physik 155:206
32. Giménez D, García-Jareño JJ, Vicente F (2002) Materiales y Procesos Electródicos I. INSDE, València, pp 65–84
33. Benito D, Gabrielli C, García-Jareño JJ, Keddam M, Perrot H, Vicente F (2003) Electrochim Acta 48:4039
34. Muñoz AG, Schultze JW (2004) Electrochim Acta 49:293
35. Schmutz P, Landolt D (1999) Electrochim Acta 45:899
36. Vergé MG, Olsson COA, Landolt D (2004) Corros Sci 46:2583
37. Hamm D, Olsson COA, Landolt D (2002) Corros Sci 44:1009
38. Beverskog B, Puigdomenech I (1997) Corros Sci 39:969
39. Nakamura M, Ikemiya N, Iwasaki A, Suzuki Y, Ito M (2004) J Electroanal Chem 566:385
40. Grden M, Klimek K, Czerwínski A (2004) J Solid State Electrochem 8:390
41. Lide DR (ed) (1995) Handbook of chemistry and physics. CRC press, New York, pp 8–58